IEEE Access
Multidisciplinary | Rapid Review | Open Access Journal

Received 2 September 2023, accepted 14 September 2023, date of publication 18 September 2023,
date of current version 28 September 2023.

Digital Object Identifier 10.1109/ACCESS.2023.3316715

RESEARCH ARTICLE

A 2.5D Broadband Non-Reciprocal Metasurface Based on Aperture-Coupled Feed Structures

QING GU, XINYUAN ZHENG, YONGGANG ZHOU, (Member, IEEE), FEIYANG SUN, AND SHAOBIN LIU, (Member, IEEE)

College of Electronic and Information Engineering, Nanjing University of Aeronautics and Astronautics, Nanjing 210016, China

Corresponding author: Shaobin Liu (lsb@nuaa.edu.cn)

This work was supported in part by the National Natural Science Foundation of China under Grant 62071221, Grant 62071442, and Grant U2141232; in part by the National Defense Science and Technology Foundation of China under Grant 2019-JCJQ-ZD-067 and Grant 2021-JCJQ-LB-047; in part by the Aeronautical Science Foundation of China under Grant 2019ZA037001; and in part by the Key Laboratory of Radar Imaging and Microwave Photonics (Nanjing University of Aeronautics and Astronautics), Ministry of Education of China, under Grant NJ20210006.

ABSTRACT In traditional non-reciprocal metasurfaces based on antenna-circuit-antenna structure, the radiation module and the non-reciprocal circuit module are coplanar, which occupies extra surface area and has the inherent defect of narrow operating bandwidth. Therefore, a new 2.5D non-reciprocal metasurface based on the aperture coupling structure is proposed to realize the separate design and broad operating bandwidth, in which the non-reciprocal circuit module is perpendicular to the radiation module. In addition, this work improves isolation to over 35 dB without affecting the radiation mode and resonance frequency. Based on multimode resonance theory, a broadband microstrip antenna is further presented to obtain a broader operating bandwidth. By exciting multiple resonant modes with similar frequencies in the resonant cavity, the relative bandwidth reaches up to 38.2%. The experimental results coincide well with the simulation results, which fully demonstrate the validity of the proposed design.

INDEX TERMS Non-reciprocity, metasurface, broadband, isolator, multimode resonance.

I. INTRODUCTION

In recent years, metasurfaces have raised great attention due to the capacity to regulate the phase [1], amplitude [2], and polarization [3] of electromagnetic waves. A variety of applications have been proposed with metasurfaces, such as harmonic wave manipulation [4], [5], [6], polarization conversion [7], and beam steering [8], [9]. Non-reciprocal devices based on metasurface, which can achieve unidirectional absorption characteristics, have an attractive future in electromagnetism. In forward transmission, the electromagnetic wave can be amplified by the active circuit. However, in reverse transmission, the electromagnetic wave cannot be transmitted through active circuit.

The traditional method to achieve non-reciprocity is based on magnetic materials, usually ferromagnetic composite materials (also known as ferrite) [10], [11]. [12] presented a ferrite-based radome that achieved a difference of more than 21 dB between the forward and reverse transmission coefficients of electromagnetic waves, exhibiting strong non-reciprocity. However, non-reciprocal devices based on ferrite materials are usually large in size and require additional magnetic field bias, making them difficult to integrate. In addition, the static magnetic fields generated can affect the normal use of the system [13], [14]. With the rise of semiconductor materials, active devices made of semiconductor materials can play the role of unidirectional amplification, and achieve non-reciprocity. In [15], Faraday rotation can be generated without a constant applied magnetic field by combining an amplifying circuit with a metasurface.

However, the above design is still limited to the use of current loops to simulate the polarized non-reciprocity generated by the Faraday rotation effect of ferrite non-reciprocal materials. [16] presented a non-reciprocal active frequency

The associate editor coordinating the review of this manuscript and approving it for publication was Giorgio Montisci.

selective surface with an antenna-circuit-antenna structure. [17] used a radiation patch and a non-reciprocal phase shifter to form a cascaded series structure that achieved deflection of the reflected beam at a specific frequency with different reflection gains. Such devices involve neither nonlinear materials nor polarization and rotation of electromagnetic waves, and achieve non-reciprocal transmission by only using conventional materials and equipment. However, the existing non-reciprocal metasurface based on antenna-circuit-antenna structure adopt the design that the radiation part is coplanar with the non-reciprocal circuit, which occupies extra surface area and makes it difficult to load more complex structures on the surface of the non-reciprocal metasurface. In addition, due to the inherent defect of microstrip antenna, the existing metasurfaces have a narrow operating bandwidth.

In this paper, a multimode resonant 2.5D broadband non-reciprocal metasurface is proposed. The radiation part and the non-reciprocal circuit part are not coplanar, but perpendicular to each other. Using this technique, the radiation part and the circuit part of the non-reciprocal metasurface are isolated, which improves the peak isolation to 35dB within 4-5.89 GHz. In addition, three resonant modes are excited, which forms the broad operating bandwidth. Finally, the measurements demonstrate that the relative bandwidth is 38.2%, the gain is 10 dB, and the isolation exceeds 35 dB.

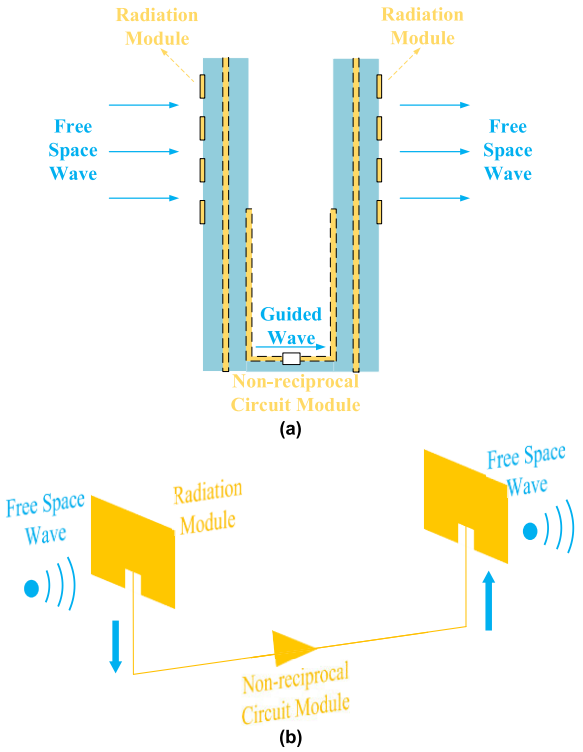

FIGURE 1. Structure of the non-reciprocal metasurface.

II. DESIGN AND SIMULATION

The designed 2.5D non-reciprocal metasurface is shown in Fig. 1. Based on the existing metasurface with the antenna-circuit-antenna structure, the non-reciprocal amplifier circuit, which was originally arranged on both sides of the metasurface and coplanar with the radiation module, is arranged on the inner side of the two layers by using aperture coupling structure. The non-reciprocal amplifier circuit is now perpendicular to the radiation module on both sides, forming a 2.5D structure. In forward transmission, the electromagnetic wave can be amplified by the active circuit. However, in reverse transmission, the electromagnetic wave cannot be transmitted through the active circuit.

In order to widen the operating bandwidth and achieve non-reciprocity, we propose a microstrip antenna based on multimode resonance and a non-reciprocity circuit. In addition, we provide detailed simulation results of the broadband microstrip antenna, non-reciprocal circuit and non-reciprocal metasurface.

A. MICROSTRIP ANTENNA BASED ON MULTIMODE RESONANCE

Microstrip antenna has a very narrow bandwidth. The bandwidth can be improved by aperture-coupled feed technique [18], [19]. [20] proposed a broadband microstrip antenna using strip-slot hybrid structure. By slotting the radiating patch and using Y-shaped microstrip feed structure, two operating modes with close resonance frequencies are excited in the resonant cavity, which are coupled together to increase the operating bandwidth.

The designed antenna is shown in Fig. 2. The antenna is composed of two substrate layers and three metal layers. Rogers 4350B is employed as substrate with dielectric constant of 3.66 and tangent loss of 0.0037. The thickness of two substrate layers is 3.25 and 0.762mm from the top to bottom. The total thickness is about 4 mm.

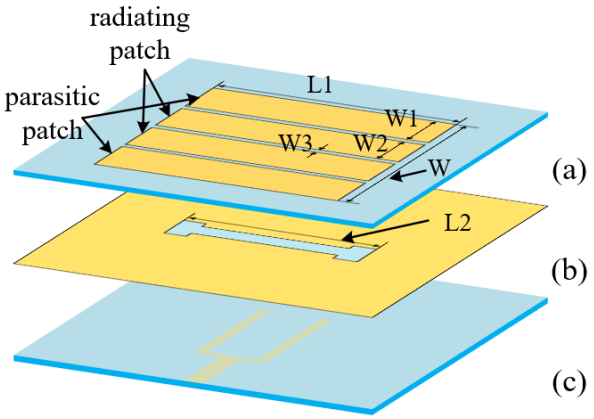

FIGURE 2. The structure of broadband microstrip antenna based on multimode resonance (a) upper layer structure (b) middle layer structure (c) bottom layer structure.

Fig. 2(a) shows the top layer structure of the microstrip antenna, which has a slit in the middle of the radiation patch and is symmetrically loaded with parasitic patches

on the outside of the radiation slot of the radiation patch; Fig. 2(b) shows the middle layer structure of the microstrip antenna, on which a metal backplane with H-shaped coupling aperture is arranged; Fig. 2(c) shows the bottom layer structure of the microstrip antenna, on which a double bias microstrip feed line is arranged. By converting the original 50 Ω microstrip feeder into a 100 Ω microstrip feeder through a power divider and symmetrically arranging it on both sides of the coupling aperture, the double-bias feed line plays the role of reducing the coupling coefficient and improving the impedance match. The labeled dimensions are provided as follows: L1 = 40mm, W = 40mm, W1 = 9.45mm, W2 = 8.9mm, W3 = 1.1mm, L2 = 31mm.

By loading slits and parasitic patches, multiple operating modes can be excited in the resonant cavity, and if the resonant frequencies are close, the multiple operating modes will be coupled together, then the operating bandwidth of the microstrip antenna can be effectively extended [21], [22], [23]. In addition, [24] and [25] show that the use of H-shaped coupling apertures provides stronger coupling and makes it easier to achieve broadband designs for antennas.

Fig. 3 shows the simulated S-parameter of the broadband microstrip antenna. As can be seen, three resonant modes are excited in the resonant cavity. The operating frequencies are 4.68GHZ, 5.24GHz and 6.05GHz respectively, and the relative bandwidth of S11 < -10 dB (VSWR<1.92) is 38.2%. The three operating modes are coupled together, which effectively broadens the operating bandwidth of the microstrip antenna. Due to the limited precision of the device parameters provided by the company, the imported S-parameters are not precise enough, and the simulation results are distorted at 4.5GHz.

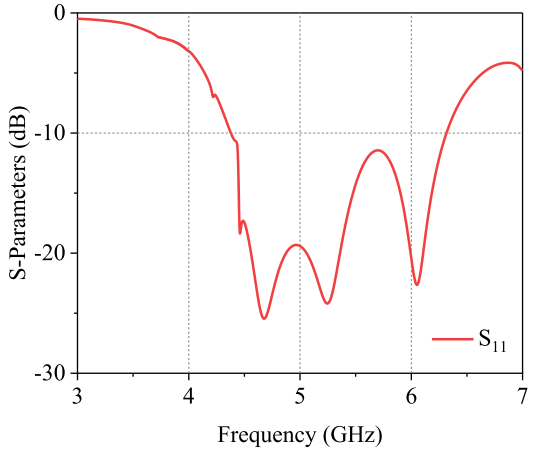

FIGURE 3. The simulated S-parameter curve of the multimode resonant broadband microstrip antenna.

According to the cavity mode theory [26], [27], [28] of the microstrip antenna, the mode with the lowest resonant frequency is the main mode TM10, as shown in Fig. 4(a), and due to the presence of the slot in the radiation patch and the parasitic patch, the antenna will excite other higher modes. In Fig. 4(b), calculated from the length of the non-radiation slot side of the parasitic patch, the second resonant point is quasi-TM20 mode, which is symmetrically excited by the slit-isolated half-side radiation patch and the parasitic patch. This mode has 2 half-cycle fields in the resonant cavity, but its electric field is synthesized from two TM10 modes, and the electric field is mutated at the patch slots. Therefore, this mode is not the strictly TM20 mode, and the final radiation mode is also synthesized from two TM10 modes. Lastly, as shown in Fig. 4(c), the third resonant frequency is the main mode TM10 of the radiation part itself without the parasitic patch. Besides, due to the inherent characteristics of the parasitic patch, the high frequency mode band will move to the low frequency [29], thus effectively expanding the operating bandwidth of the antenna. Fig.5 shows the simulated e-field distributions of the Antenna.

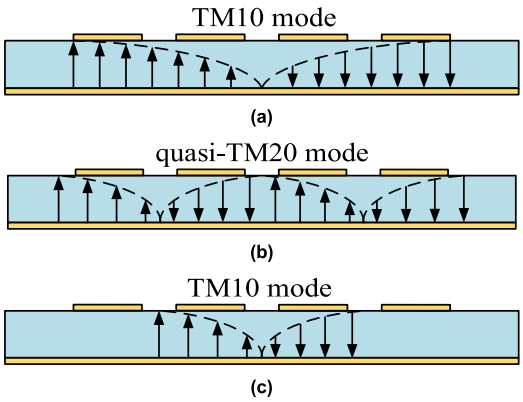

FIGURE 4. The resonant electric field distribution of the Antenna (a) first resonance point (b) second resonance point (c) third resonance point.

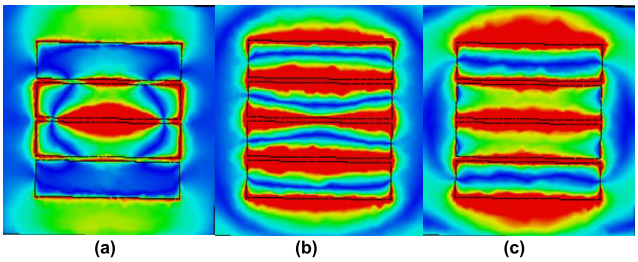

FIGURE 5. The simulated e-field distributions of the Antenna (a) first resonance point (b) second resonance point (c) third resonance point.

B. NON-RECIPROCAL AMPLIFIER CIRCUIT

The structure of the non-reciprocal circuit in Fig. 6 can be divided into two parts: DC path and RF path. The DC path generates bias voltage for the amplifier and stabilizes its operating state. The RF path serves as the RF signal transmission channel and generates non-reciprocity. In forward transmission, the RF signal can be amplified by the active circuit. However, in reverse transmission, the RF signal cannot be transmitted through active circuit. Due to the blocking of inductor L, the RF signal is confined within the RF path

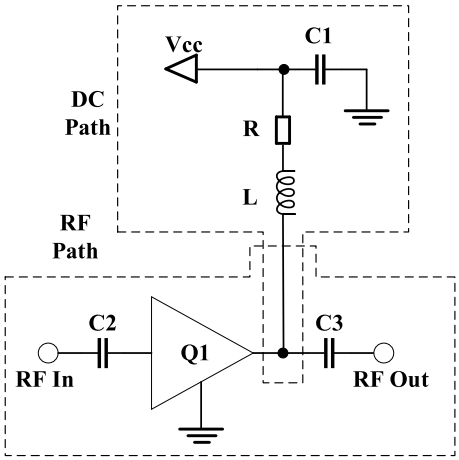

FIGURE 6. Structure of the non-reciprocal amplifier circuit.

and cannot enter the DC path. In addition, the presence of inductor L avoids the impedance change generated by the bias line of the DC path on the transmission line of the RF path, which ensures the normal operation of the RF path. The passive components of the non-reciprocal circuit are as follows: C1 = 18nF, C2 = 56pF, C3 = 56pF, R = 24 Ω, L = 39nH.

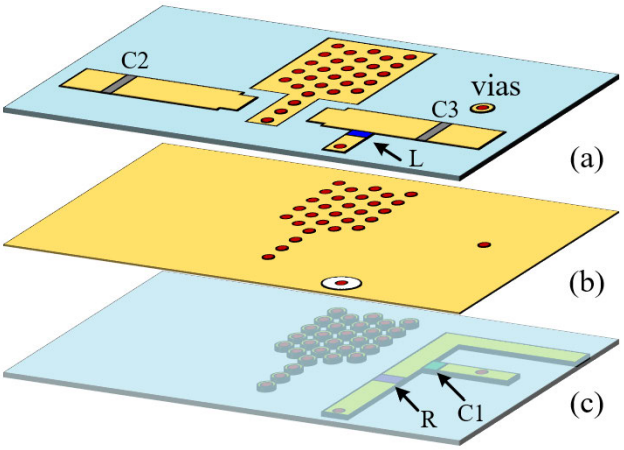

FIGURE 7. Physical model of the non-reciprocal amplifier circuit (a) top layer structure (b) middle layer structure (c) bottom layer structure.

The physical model of the non-reciprocal amplifier circuit obtained from the above design idea is shown in Fig. 7. The physical structure is also composed of two layers of substrate and three layers of metal. The dielectric substrate material is Rogers 4350B with the thickness of 0.732 mm. The yellow part of the figure is copper foil and the red part is metallized vias. Fig. 7(a) shows the top structure of the non-reciprocal circuit, with pads of the MMIC amplifier in the center, which achieves good grounding and heat dissipation. The gray parts represent capacitors C2 and C3 and the blue part represents inductor L; Fig. 7(b) shows the middle structure of the circuit, where the whole metal ground is arranged; Fig. 7(c) shows the bottom structure of the circuit, with capacitor C1 in green and resistor R in purple. In addition, the bottom layer leads two DC bias lines for connecting the external power supply.

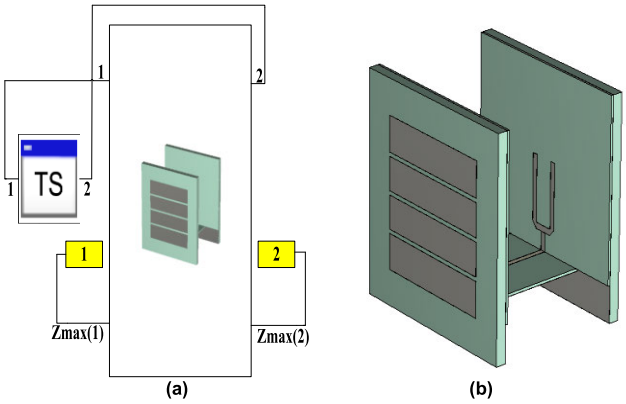

FIGURE 8. The non-reciprocal metasurface in CST (a) non-reciprocal circuit model (b) non-reciprocal metasurface model.

After selecting the appropriate devices according to the circuit designed in Fig. 6 and Fig. 7, the simulation of DC circuit and the design of matching circuit are performed. Finally, the overall circuit design is completed and the obtained non-reciprocal circuit model is shown in Fig. 8(a).

The simulations for the non-reciprocal amplifier circuit are performed in ADS and CST Studio Suite and the results are recorded. As can be seen in Fig. 9, the designed non-reciprocal circuit has flat gain and strong non-reciprocity, with a gain of more than 10 dB and reverse isolation of more than 20 dB. In ADS and CST, the S11 curves do not match. In ADS, the non-reciprocal circuits are in the form of schematic. However, in CST, the non-reciprocal circuits take the form of the physical model. Unlike the schematic, in the physical model, there is coupling between the transmission line and the amplifier pads, which creates an unexpected capacitance that increases the reflection coefficient at one port, which does not match the simulation results in ADS. Apart from this, the simulation results in ADS and CST coincide well, which fully demonstrate the validity of the proposed method and design.

C. THE NEW BROADBAND NON-RECIPROCAL METASURFACE

The radiation module and the circuit module of the metasurface are modeled and spliced in CST. Fig. 8(b) shows the model of non-reciprocal metasurface in CST. The field-circuit co-simulation in CST software is applied in the simulations. As can be seen from Fig. 10, the broadband non-reciprocal metasurface has a passband frequency range of 4GHz-5.89GHz, with good rectangular coefficient and sharp cutoff characteristics. A forward 15dB gain and 35dB reverse isolation are achieved in its passband, and comparing its forward and reverse transmission coefficients, the broadband metasurface shows strong non-reciprocity.

The simulated radiation patterns of the 4 × 4 metasurface is shown in Fig. 11. It can be seen that at 4.6 GHz, the

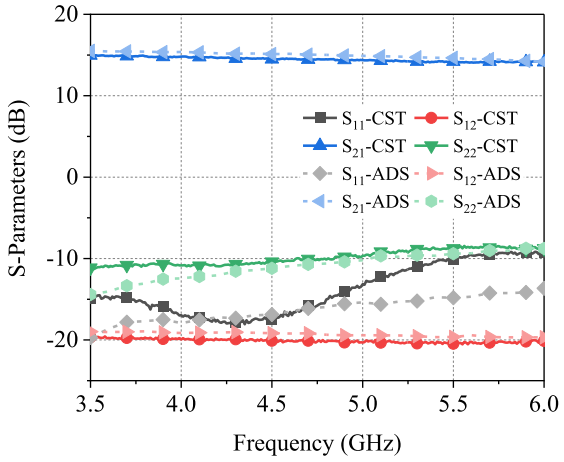

FIGURE 9. Comparison of simulation results in ADS and CST.

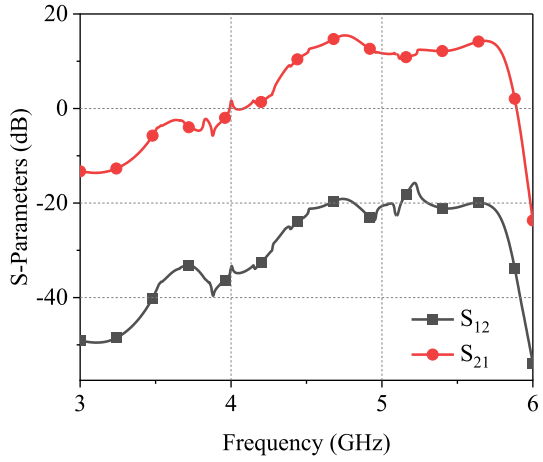

FIGURE 10. The simulated S-parameters of the metasurface.

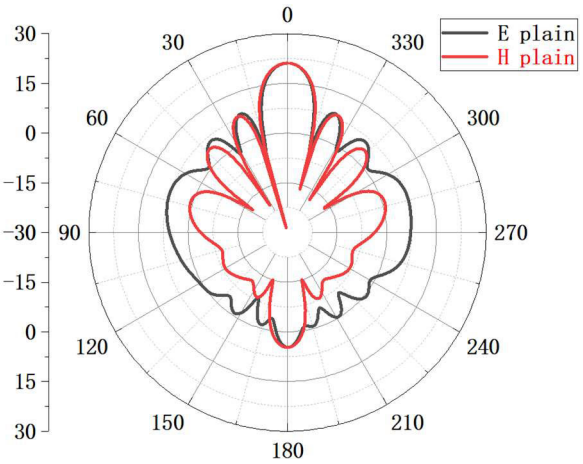

FIGURE 11. The simulated radiation pattern of the 4 × 4 non-reciprocal metasurface.

non-reciprocal metasurface has a good directionality, with a main flap amplitude of 21 dB and a low side flap, which can effectively receive the electromagnetic waves radiated from outside.

III. RESULTS AND DISCUSSION

To experimentally verify the proposed method and design, the non-reciprocal amplifier circuit and the non-reciprocal metasurface are fabricated. The micrograph of the non-reciprocal circuit is shown in Fig. 12. Figure 12(a) shows amplification circuit on the front. Figure 12(b) shows the bias circuit on the back. The non-reciprocal circuit's RF In and RF Out are connected to the Agilent N5245A vector network analyzer by soldering on 50Ω SMA RF coaxial connectors, and the DC bias line is connected to the DC power supply.

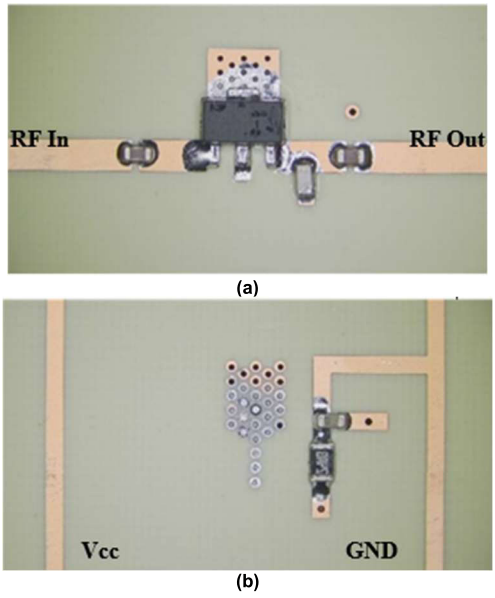

FIGURE 12. Micrographs of non-reciprocal circuit (a) amplifier circuit (b) bias circuit.

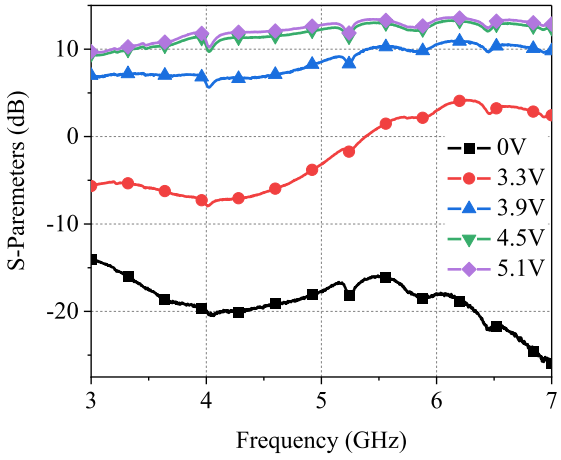

FIGURE 13. Transmission coefficients at different voltages.

Adjust the output voltage of the DC power supply and record the non-reciprocal circuit transmission coefficient at various output voltages. The gain of the non-reciprocal circuit stops increasing with the bias voltage when the output of the DC power source hits 5.1V, as shown in Fig. 13, and

the MMIC amplifier enters the full bias state. The MMIC amplifier can ensure that amplifier parameters are consistent with the simulation model when it reaches full bias state.

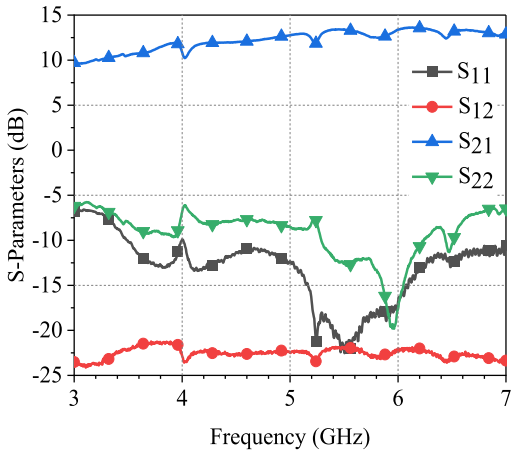

FIGURE 14. S-parameter of the non-reciprocal circuit at full bias.

The measured S-parameter results at full bias state are given in Fig. 14. As can be seen, the gain of the non-reciprocal circuit is basically flat in the operating band, generating a gain of more than 10 dB and reverse isolation of more than 35 dB, which coincides well with the results obtained from the simulation. However, it also reflects the low transmission coefficient and strong reflection coefficient of the non-reciprocal circuit, as well as the resonance phenomenon at specific frequency points. It is assumed that the reason for this phenomenon is that when the SMA RF coaxial connector is connected to the non-reciprocal circuit, the coupling connection is made between the outer conductor of the connector and the metal ground of the non-reciprocal circuit. Due to the error in the welding of the inner conductor of the coaxial connector and the microstrip line, which increases the loss, the coupling efficiency at the connection is affected. In addition, because the two layers are connected by using press-fit technique, the plates produce irregular bending deformation, which leads to a certain error between the experimental results and the simulation results. Other than that, the designed circuit generally exhibits good non-reciprocity.

The fabricated metasurface sample is composed of 4×4 non-reciprocal metasurfaces proposed above, as presented in Fig. 15(a). The two layers of dielectric substrate of the radiation module are fixed by 13 nylon bolts and nuts, the non-reciprocal circuit part is plugged together through the space reserved for the dielectric substrate of the inner layer of the radiation part, and the microstrip lines of the non-reciprocal circuit part are connected to the microstrip feeder of the radiation part by using solder. Fig.15(a) also shows the circuit module of the non-reciprocal metasurface, which connects the radiation modules on both sides. The above figure is the amplifier circuit, while the below one is the feeder circuit. The experimental environment for S-parameter measurement is shown in Fig. 15(b).

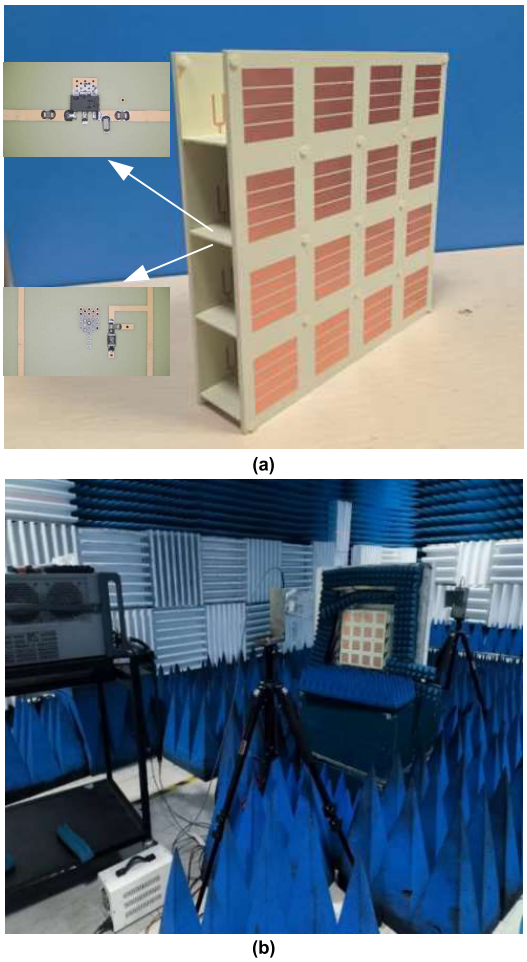

FIGURE 15. Broadband non-reciprocal metasurface based on aperture-coupled feed structures (a) all-length figure of the metasurface (b) the experimental environment.

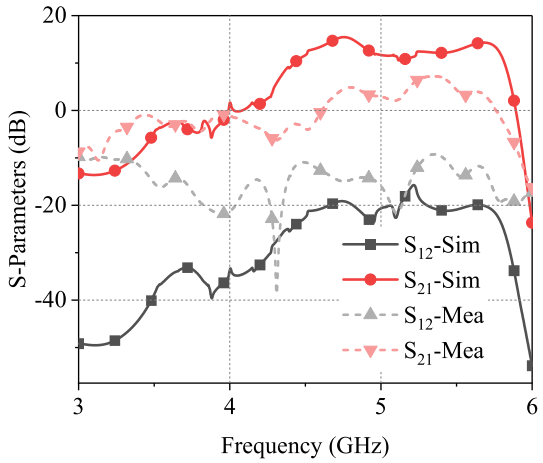

FIGURE 16. Comparison of experiment and simulation of the non-reciprocal metasurface.

The comparison of experimental results and simulation results is shown in Fig. 16. The low-frequency part of the measured results, due to the low frequency and long

wavelength of the electromagnetic wave, produces a bypass of the test module, making the measured reverse transmission coefficients high in the 3-4 GHz range. In addition, the non-reciprocal circuit module is plugged into the radiation module, and there is an unavoidable air gap of 0.05-0.1 mm between the two modules, which makes the two modules produce a large loss at the connection. For the high-frequency part, because the non-reciprocal metasurface adopts a spliced 2.5D structure instead of a one-piece structure, the radiation module and the non-reciprocal circuit module are coupled, the transmission line at the connection is discontinuous, mutation occurs, and there are inevitably some solder residues at the connection, which generates a large loss. In addition, since the metasurface fabricated is only 4×4 in size, the electromagnetic wave produces a large bypass. For non-reciprocal metasurfaces, the spliced 2.5D structure is not an ideal structure compared to the conventional one-piece structure due to the limitations of the existing technology. Overall, the metasurface exhibits good non-reciprocity.

As can be seen from Table 1, compared with the existing one-piece non-reciprocal metasurface based on antenna-circuit-antenna structures, the new 2.5D broadband non-reciprocal metasurface proposed in this paper significantly broadens the operating bandwidth and has better non-reciprocity due to the separation of the radiation part and the non-reciprocal circuit part.

TABLE 1. Comparison between the designed metasurface and existing works.

Ref.	Structure	Isolation/dBi	Gain/dBi	BW/GHz
[16]	one-piece	27	10	5.8-6 (3.3%)
[17]	one-piece	22	19	5.7-6 (5.12%)
[30]	one-piece	19.2	8.5	4.88-5.19 (6.15%)
This work	2.5D	35	15	4-5.89 (38.2%)

IV. CONCLUSION

In this paper, a new 2.5D broadband non-reciprocal metasurface based on aperture-coupled feed structure is designed, in which the non-reciprocal circuit part is arranged perpendicular to the radiation part on both sides, forming a 2.5D structure. Through this work, the radiation module and the non-reciprocal circuit module are isolated, which reduces the difficulties of design and effectively improves the isolation. In addition, a new broadband microstrip antenna based on multimode resonance theory and a new non-reciprocal amplifier circuit are proposed, achieving a 38.2% relative bandwidth, a gain of 15 dB and reverse isolation of more than 35 dB in the passband, demonstrating good reciprocity.

The non-reciprocal metasurface proposed in this paper realizes the unidirectional transmission of electromagnetic waves, which can play a role in electromagnetic stealth. In addition, the operating bandwidth of the metasurface is close to the commercial bandwidth of 5G. The proposed metasurface could amplify 5G signals indoors to ensure 5G communication quality, which could contribute to the construction of 5G. By replacing different non-reciprocal circuits and radiation modules, more complex functions can be realized, providing the basis for the new structure with the separate and easy design of the non-reciprocal metasurface.

REFERENCES

[1] A. Arbabi, Y. Horie, M. Bagheri, and A. Faraon, "Dielectric metasurfaces for complete control of phase and polarization with subwavelength spatial resolution and high transmission," *Nature Nanotechnol.*, vol. 10, no. 11, pp. 937–943, Aug. 2015.
[2] L. Liu, X. Zhang, M. Kenney, X. Su, N. Xu, C. Ouyang, Y. Shi, J. Han, W. Zhang, and S. Zhang, "Broadband metasurfaces with simultaneous control of phase and amplitude," *Adv. Mater.*, vol. 26, no. 29, pp. 5031–5036, Aug. 2014.
[3] Y. Zhao and A. Alú, "Manipulating light polarization with ultrathin plasmonic metasurfaces," *Phys. Rev. B, Condens. Matter*, vol. 84, no. 20, Nov. 2011, Art. no. 205428.
[4] J. Y. Dai, J. Yang, W. Tang, M. Z. Chen, J. C. Ke, Q. Cheng, S. Jin, and T. J. Cui, "Arbitrary manipulations of dual harmonics and their wave behaviors based on space-time-coding digital metasurface," *Appl. Phys. Rev.*, vol. 7, no. 4, Dec. 2020, Art. no. 041408.
[5] J. Y. Dai, L. X. Yang, and M. Z. Chen, "High-efficiency synthesizer for spatial waves based on space-time-coding digital metasurface," *Laser Photon. Rev.*, vol. 14, no. 6, May 2020, Art. no. 1900133.
[6] C. Zhang, J. Yang, L. X. Yang, J. C. Ke, M. Z. Chen, W. K. Cao, M. Chen, Z. H. Wu, J. F. Chen, Q. Cheng, and T. J. Cui, "Convolution operations on time-domain digital coding metasurface for beam manipulations of harmonics," *Nanophotonics*, vol. 9, no. 9, pp. 2771–2781, Jul. 2020.
[7] J. C. Ke, J. Y. Dai, and M. Z. Chen, "Linear and nonlinear polarization syntheses and their programmable controls based on anisotropic time-domain digital coding metasurface," *Small Struct.*, vol. 2, no. 1, Jan. 2021, Art. no. 2000060.
[8] L. Bao, Q. Ma, and R. Y. Wu, "Programmable reflection-transmission shared-aperture metasurface for real-time control of electromagnetic waves in full space," *Adv. Sci.*, vol. 8, no. 15, May 2021, Art. no. 2100149.
[9] G. Castaldi, L. Zhang, and M. Moccia, "Joint multi-frequency beam shaping and steering via space–time-coding digital metasurfaces," *Adv. Funct. Mater.*, vol. 31, no. 6, Oct. 2020, Art. no. 2007620.
[10] J. D. Adam, L. E. Davis, G. F. Dionne, E. F. Schloemann, and S. N. Stitzer, "Ferrite devices and materials," *IEEE Trans. Microw. Theory Tech.*, vol. 50, no. 3, pp. 721–737, Mar. 2002.
[11] H. Dötsch, N. Bahlmann, and O. Zhuromskyy, "Applications of magneto-optical waveguides in integrated optics," *J. Opt. Soc. Amer. B, Opt. Phys.*, vol. 22, no. 1, pp. 240–253, 2005.
[12] A. Parsa, T. Kodera, and C. Caloz, "Ferrite based non-reciprocal radome, generalized scattering matrix analysis and experimental demonstration," *IEEE Trans. Antennas Propag.*, vol. 59, no. 3, pp. 810–817, Mar. 2010.
[13] Y. Zhang, Q. Y. Du, and C. T. Wang, "Monolithic integration of broadband optical isolators for polarization-diverse silicon photonics," *Optica*, vol. 6, pp. 473–478, Apr. 2019.
[14] H. Dong, J. R. Smith, and J. L. Young, "A wide-band, high isolation UHF lumped-element ferrite circulator," *IEEE Microw. Wireless Compon. Lett.*, vol. 23, no. 6, pp. 294–296, Jun. 2013.
[15] Z. Wang, Z. Wang, J. Wang, B. Zhang, J. Huangfu, J. D. Joannopoulos, M. Soljačić, and L. Ran, "Gyrotropic response in the absence of a bias field," *Proc. Nat. Acad. Sci. USA*, vol. 109, no. 33, pp. 13194–13197, Aug. 2012.
[16] S. Taravati, B. A. Khan, and S. Gupta, "Nonreciprocal nongyrotropic magnetless metasurface," *IEEE Trans. Antennas Propag.*, vol. 65, no. 7, pp. 3589–3597, Jul. 2017.
[17] S. Taravati and G. V. Eleftheriades, "Full-duplex reflective beamsteering metasurface featuring magnetless nonreciprocal amplification," *Nature Commun.*, vol. 12, no. 1, pp. 1–11, Jul. 2021.
[18] A. Foudazi, T. E. Roth, and M. T. Ghasr, "Aperture-coupled microstrip patch antenna fed by orthogonal SIW line for millimeter wave imaging applications," *IET Microw., Antennas Propag.*, vol. 11, no. 6, pp. 811–817, Mar. 2016.
[19] J. Wei, X. Jiang, and L. Peng, "Ultrawideband and high-gain circularly polarized antenna with double-Y-shape slot," *IEEE Antennas Wireless Propag. Lett.*, vol. 16, pp. 1508–1511, 2017.

[20] W. Sun, Y. Li, Z. Zhang, and Z. Feng, "Broadband and low-profile microstrip antenna using strip-slot hybrid structure," *IEEE Antennas Wireless Propag. Lett.*, vol. 16, pp. 3118–3121, 2017.
[21] K. H. Kim, S. B. Cho, and Y. J. Park, "Novel planar ultra wideband stepped-fat dipole antenna," in *Proc. IEEE Conf. Ultra Wideband Syst. Technol.*, Nov. 2003, pp. 508–512.
[22] C.-K. Wu and K.-L. Wong, "Broadband microstrip antenna with directly coupled and parasitic patches," *Microw. Opt. Technol. Lett.*, vol. 22, no. 5, pp. 348–349, Sep. 1999.
[23] K. M. Luk, C. L. Mak, Y. L. Chow, and K. F. Lee, "Broadband microstrip patch antenna," *Electron. Lett.*, vol. 34, no. 15, pp. 1442–1443, Jul. 1998.
[24] K. L. Wong, H. C. Tung, and T. W. Chiou, "Broadband dual-polarized aperture-coupled patch antennas with modified H-shaped coupling slots," *IEEE Trans. Antennas Propag.*, vol. 50, no. 2, pp. 188–191, Feb. 2002.
[25] J. W. Kim and J. S. Jeon, "Wideband dual-polarized microstrip antenna with H-shaped coupling slot," *J. Korea Soc. Comput. Inf.*, vol. 19, no. 4, pp. 71–79, Apr. 2014.
[26] Y. T. Lo, D. Solomon, and W. F. Richards, "Theory and experiment on microstrip antennas," *IEEE Trans. Antennas Propag.*, vol. AP-27, no. 2, pp. 137–145, Mar. 1979.
[27] J. Q. Howell, "Microstrip antennas," *IEEE Trans. Antennas Propag.*, vol. AP-23, no. 1, pp. 90–93, Jan. 1975.
[28] W. F. Richards, Y. T. Lo, and D. D. Harrison, "An improved theory of microstrip antennas with applications," *IEEE Trans. Antennas Propag.*, vol. AP-29, no. 1, pp. 38–46, Jan. 1981.
[29] Y. M. Pan, P. F. Hu, and X. Y. Zhang, "A low-profile high-gain and wideband filtering antenna with metasurface," *IEEE Trans. Antennas Propag.*, vol. 64, no. 5, pp. 2010–2016, May 2016.
[30] T. Lou, X. X. Yang, and G. He, "Dual-polarized nonreciprocal spatial amplification active metasurface," *IEEE Antennas Wireless Propag. Lett.*, vol. 20, no. 9, pp. 1789–1793, Sep. 2021.

QING GU was born in Jiangsu, China, in 2001. He is currently pursuing the B.S. degree in electronic science and technology with the College of Electronic and Information Engineering, Nanjing University of Aeronautics and Astronautics, Nanjing, China. His research interests include frequency-selective surface, antenna design, and microwave circuits.

XINYUAN ZHENG was born in Liaoning, China, in 1998. He is currently pursuing the M.S. degree with the College of Electronic and Information Engineering, Nanjing University of Aeronautics and Astronautics, Nanjing, China. His research interest includes frequency-selective surface.

YONGGANG ZHOU (Member, IEEE) was born in Neijiang, China, in 1972. He received the B.S., M.S., and Ph.D. degrees from the Nanjing University of Aeronautics and Astronautics, in 1993, 2000, and 2006, respectively. He is currently an Associate Professor with the College of Electronic Information Engineering, Nanjing University of Aeronautics and Astronautics. His research interests include reconfigurable antenna, tightly coupled array, and RF simulation system technology.

FEIYANG SUN was born in Anhui, China, in 1999. He received the B.S. degree in communication engineering from the University of Science and Technology Beijing, Beijing, China, in 2021. His research interests include electromagnetic metasurface, antenna design, radio frequency, and microwave circuits.

SHAOBIN LIU (Member, IEEE) received the Ph.D. degree in electronics science and technology from the National University of Defense Technology, Changsha, China, in 2004. He is currently a Professor in electromagnetic and microwave technology with the Nanjing University of Aeronautics and Astronautics, Nanjing, China. His research interests include plasma stealthy antennas, microwave, radio frequency, and electromagnetic compatibility.